JTTEE5 4:287-296

Prediction of Powder Particle Behavior during High-Velocity Oxyfuel Spraying

V.V. Sobolev, J.M. Guilemany, and J.A. Calero

A mathematical model is developed to predict particle velocity and temperature during high-velocity oxyfuel (HVOF) spraying. This model accounts for internal heat conduction in powder particles; particle heating, fusion, cooling, and solidification; the influence of particle morphology on thermal behavior; and the composite structure of the particles. Analytical results are obtained that describe particle velocity and temperature variations. The dependence of fluid velocity on particle density and volume fraction is shown. The results agree with empirically established HVOF spraying practice.

1. Introduction

HIGH-VELOCITY oxyfuel (HVOF) spraying has developed over the last decade and is a viable process for many coating applications (Ref 1, 2). To improve the technology of HVOF spraying and to establish its optimal conditions, both the mechanical and the thermal behavior of the powder particles must be studied; such study is one of the main elements of process control development (Ref 2). Mathematical simulation is an effective tool to approach this problem.

The objective of this paper is to present a realistic prediction model that takes into account the characteristic features of HVOF spraying. We further develop the results presented in Ref 3 and 4 by considering the fluid/solid particle interactions in the flame and the full thermal evolution of the powder particles, including their heating, melting, cooling, and solidification during movement toward the substrate.

2. Model Description

Different mathematical models that describe the behavior of powder particles during plasma spraying have been developed in the last decade (Ref 2, 5, 6). Similar problems concerning HVOF spraying were considered in Ref 7, but that model did not account for several important features of HVOF spraying, such as fluid velocity dependence on particle density. Fluid and powder particles in the combustion flame cannot be taken as separate and independent substances but must be considered as two elements of a fluid/solid particle mixture, each component having its own particular properties (Ref 8).

It is also necessary to take into account the considerable variation of fluid velocity at the spraying distance, the composite structure of the particles (consisting of carbides and binding elements), the relatively small influence of the Knudsen discontinuum effect on heat and momentum transfer, the thermal behavior of particles inside the spraying gun of the HVOF system, the particle morphology, and the full description of the thermal state of powder particles during HVOF spraying, which generally includes their heating, melting, cooling, and solidification. In addition to spherical particles, we consider cylindrical particles, which correspond approximately to either the initial form of solid particles or to a form that can arise due to the in-flight deformation of liquid particles. We consider the particles moving along the centerline of the fluid flow, because these particles are the prime contributors to coating formation (Ref 1, 5-7).

Keywords: high-velocity oxyfuel spraying, mathematical simulation, mechanical movement, powder particle, thermal evolution

V.V. Sobolev, J.M. Guilemany, and **J.A. Calero,** Physical Metallurgy—Materials Science, Department of Chemical Engineering and Metallurgy, University of Barcelona, 08028 Barcelona, Spain

2.1 *Fluid Parameters*

The axial distance of particle movement in the HVOF spraying process is presented in Fig. 1. The origin of the longitudinal coordinate z coincides with the point of powder particle acceleration and temperature increase due to the combustion caused by the chemical reaction of the combustion gas (propane, in our case) with oxygen.

The fluid velocity V_f increases and the temperature T_f diminishes with distance from the gun throat ($z = 0$) to its exit ($z = l$)—from V_{f0} to V_{fp} and from T_{f0} to T_{fp}, respectively (Ref 9). The fluid expansion outside the gun leads to a further increase in velocity and a decrease in temperature in the supersonic flame arising at the gun exit in the form of shock waves (shock diamonds).

The increasing fluid velocity achieves its maximum value V_{fm} at the point $z = z_m$, corresponding to the end of the flame, and then decreases toward the substrate, taking the values V_{fc} at the characteristic spraying distance $z = z_c$ and V_{fs} at the substrate surface $z = L$. Here, the additional distance L-z_c is introduced to carry out the mathematical simulation of the full thermal behavior of powder particles, including their cooling and possible solidification if the substrate distance from the gun exit significantly exceeds that of the combustion flame. The fluid temperature decreases from the gun exit, taking the value T_{fm} at the flame end ($z = z_m$); then it continues to diminish and attains the values T_{fc} and T_{fs} at $z = z_c$ and $z = L$, respectively.

By means of linear interpolation of the experimental data (Ref 4), the fluid velocity and the fluid temperature can be presented as functions of z:

$$V_f = V_{f0} + (V_{fp} - V_{f0})zl^{-1}, 0 \le z \le l \quad \text{(Eq 1)}$$

$$V_f = (z_m - l)^{-1}[(V_{fm} - V_{fp})z + V_{fp}z_m - V_{fm}l], l \le z \le z_m \quad \text{(Eq 2)}$$

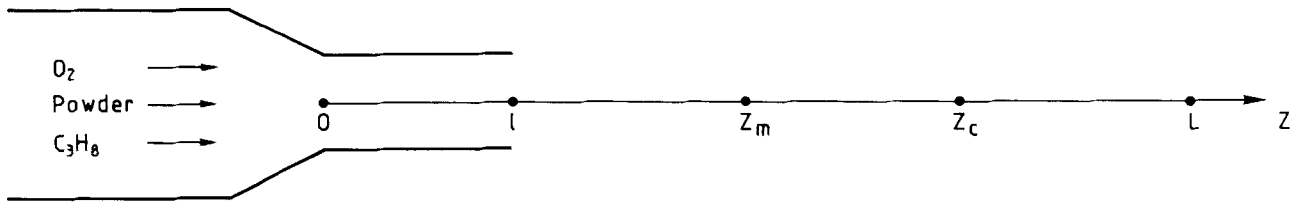

Fig. 1 Axial distance of particle movement in the HVOF spraying process

$$V_f = (z_c - z_m)^{-1}[(V_{fc} - V_{fm})z + V_{fm}z_c - V_{fc}z_m],\ z_m \le z \le z_c \quad \text{(Eq 3)}$$

$$V_f = (L - z_c)^{-1}[(V_{fs} - V_{fc})z + V_{fc}L - V_{fs}z_c],\ z_c \le z \le L \quad \text{(Eq 4)}$$

$$T_f = T_{f0} - (T_{f0} - T_{fp})zl^{-1},\ 0 \le z \le l \quad \text{(Eq 5)}$$

$$T_f = (z_m - l)^{-1}[(T_{fm} - T_{fp})z + T_{fp}z_m - T_{fm}l],\ l \le z \le z_m \quad \text{(Eq 6)}$$

$$T_f = (z_c - z_m)^{-1}[(T_{fc} - T_{fm})z + T_{fm}z_c - T_{fc}z_m],\ z_m \le z \le z_c \quad \text{(Eq 7)}$$

$$T_f = (L - z_c)^{-1}[(T_{fs} - T_{fc})z + T_{fc}L - T_{fs}z_c],\ z_c \le z \le L \quad \text{(Eq 8)}$$

For particle behavior outside the gun in HVOF spraying, approximation of the fluid velocity in this region is very important. In accordance with experimental data (Ref 4), the following formulas for V_f obtained with squared interpolation were also used in the interval $l \le z \le z_c$:

$$V_f = Az^2 + Bz + C,\ l \le z \le z_c \quad \text{(Eq 9)}$$

where

$$A = -[(z_c - l)(z_c - z_m)(z_m - l)]^{-1}[(V_{fp} - V_{fc})(z_m - l) + (V_{fm} - V_{fp})(z_c - l)]$$

$$B = (z_m - l)^{-1}[V_{fm} - V_{fp} - a(z_m^2 - l^2)],\ C = V_{fp} - Bl - Al^2$$

In general, in a fluid/solid particle medium with a volume fraction of η of these particles, an interaction occurs between the particles and the fluid. Taking into account that $\eta << 1$, V_f can be represented in a series expansion with respect to η:

$$V_f = V_f^{(0)} + \eta V_f^{(1)} + O(\eta^2) \quad \text{(Eq 10)}$$

where $V_f^{(0)}$ corresponds to $\eta = 0$ and is equal to the functions determined with Eq 1 to 4 and Eq 9. Substituting Eq 10 in the corresponding momentum transfer equation of gaseous phase within the two-fluid approach, where gas and particulate phases are considered as two interactive fluids (Ref 8), yields:

$$\frac{dV_f^{(1)}}{dt} = \frac{a_1\eta}{1-\eta}(V_p - V_f^{(0)}),\ a_1 = \frac{18\mu_f}{d_p^2\rho_f} \quad \text{(Eq 11)}$$

Because in our case $dz = V_p dt$, Eq 11 gives:

$$\frac{dV_f^{(1)}}{dz} = \frac{a_1\eta}{1-\eta}\left(1 - \frac{V_f^{(0)}}{V_p}\right) \quad \text{(Eq 12)}$$

Thus, by determining $V_f^{(1)}$ from Eq 12 and substituting it in Eq 10, we obtain V_f by taking into account fluid/particle interaction.

2.2 *Momentum Transfer*

In general, gas/solid particle transport phenomena should be considered within the framework of the suspension flow in which the fluid/particle medium is taken as a single one with its own particular properties (Ref 8). Using this approach, the equation of motion of the spherical particles in HVOF spraying can be presented as (Ref 2, 8, 10):

$$\frac{dV_p}{dt} = \frac{3}{4}\frac{C_D}{d_p}\frac{\rho_f}{\rho_p}(V_f - V_p)|V_f - V_p| + a_2\eta(1 + 0.15Re^{0.687})(V_f - V_p) \quad \text{(Eq 13)}$$

$$C_D = (23.707/Re)(1 + 0.165\,Re^{2/3} - 0.5\,Re^{-0.1}),\quad 0.15 \le Re \le 500 \quad \text{(Eq 14)}$$

where

$$Re = d_p|V_p - V_f|\bar{\rho}_f\bar{\mu}_f^{-1},\ a_2 = 18\mu_f(d_p^2\rho_p)^{-1}$$

When $\eta = 0$, from Eq 13 we obtain an equation that is widely used (Ref 2):

$$\frac{dV_p}{dt} = \frac{3}{4}\frac{C_D}{d_p}\frac{\rho_f}{\rho_p}(V_f - V_p)|V_f - V_p| \quad \text{(Eq 15)}$$

The second term on the right side of Eq 13 represents the force of interaction between fluid and solid particles. Because these particles possess inertia, they are unable to follow the smallest-scale motions of the turbulence. As a result, relative motion and interaction between the particles and the fluid arise (Ref 8). Generally, this term also introduces drag correction factors, which take into account the influence of the gun walls on particle movement caused by fluid deceleration near these walls and the increase in relative velocity between particles and fluid. The correction factors depend on the ratio between the particle radius and the distance between the particle and the wall (Ref 8). Considering that the region of their influence is considerably smaller than the region of fluid/particle movement inside the gun, they are neglected.

The initial condition for solving the equation of motion that corresponds to $t = 0$ is

$$V_p(0) = V_{p0} \quad \text{(Eq 16)}$$

Because the initial position z_0 of the particle is known, its axial location z at any moment of time is given by:

$$z(t) = \int_0^t V_p(t)dt \quad \text{(Eq 17)}$$

The initial powder particles include not only spherical types but also stretched particles, the form of which can be approximated as cylindrical with length h. This form can also arise as a result of deformation of the liquid drops appearing after in-flight melting of the powder particles in the flame.

The drag coefficient of nonspherical particles depends on their sphericity, φ, which is the surface area of a sphere of equivalent volume divided by the particle surface area (Ref 8). If $h/R_p = 4.5$, the drag coefficients of spherical and cylindrical particles are equal ($\varphi = 1$). When, for example, $h/R_p = 6$, $\varphi = 0.9$. A cylindrical particle generally moves under some angle with respect to the direction of motion. Let this angle be 30°. Using a value of $h = 6R_p$ and the results of Ref 8, the momentum transfer for cylindrical particles can be approximately described with the equations of motion (Eq 13 and 15). It should be emphasized that in this case these equations, although realistic, are only for illustrative purposes.

Equations 13 and 15 describe the motion of rigid spherical particles during HVOF spraying. After fusion, a particle becomes at least partially liquid and the Hadamard-Rybczynski equation describing the motion of a liquid particle usually should be used. In this case, the drag coefficient, c_D, is multiplied by the factor $(2 + 3x)(1 + x)^{-1}$, where $x = \mu_p\mu_f^{-1}$ (Ref 10). In our case, $x \approx 50$ and thus the viscous liquid sphere has essentially the same drag as a rigid one (Ref 10). Therefore Eq 13 and 15 can be used to describe the mechanical behavior of a particle both before and after it melts during HVOF spraying.

2.3 *Heat Transfer*

Particle thermal behavior during HVOF spraying is described by the following heat conduction equation:

$$\rho_p C_p \frac{\partial T_p}{\partial t} = \frac{1}{r^n}\frac{\partial}{\partial r}\left(r^n \lambda_p \frac{\partial T_p}{\partial r}\right), 0 \le r \le R_p \quad \text{(Eq 18)}$$

The powder particle temperature T is a function of time t and radial coordinate r. The boundary condition of the thermal field symmetry is introduced, and the boundary condition describing gas/particle heat exchange occurs at the particle surface. These boundary conditions are described by:

$$\frac{\partial T_p}{\partial r}(0,t) = 0 \quad \text{(Eq 19)}$$

$$\lambda_p \frac{\partial T_p}{\partial r}(R_p,t) = \alpha[T_f - T_p(R_p,t)] \quad \text{(Eq 20)}$$

In the initial moment of time ($t = 0$), the particle temperature is T_{p0}:

$$T_p(r,0) = T_{p0} \quad \text{(Eq 21)}$$

The coefficient of heat transfer, α, in Eq 20 can be determined using the Ranz-Marshall semiempirical equation (Ref 2):

$$Nu = \frac{\alpha d_p}{\lambda_f} = 2 + 0.6Re^{1/2}Pr^{1/3},\ Pr = \bar{c}_f \bar{\mu}_f \bar{\lambda}_f^{-1} \quad \text{(Eq 22)}$$

To calculate Re, Nu, and Pr, the integral mean values of ρ_f, μ_f, c_f, and λ_f are used in the temperature interval $T_{ps} \le T \le T_f$:

$$\bar{\rho}_f = b_1 \int_{T_{ps}}^{T_f} \rho_f dT,\ \bar{\mu}_f = b_1 \int_{T_{ps}}^{T_f} \mu_f dT,\ \bar{c}_f = b_1 \int_{T_{ps}}^{T_f} c_f dT,$$

$$\bar{\lambda}_f = b_1 \int_{T_{ps}}^{T_f} \lambda_f dT, b_1 = (T_f - T_{ps})^{-1} \quad \text{(Eq 23)}$$

In general, during HVOF spraying the particle is heated and its surface attains the melting temperature. Then the melting front propagates toward the particle center until it is fully molten. Afterward the particle can be heated further and then cooled. In the process of cooling, the solidification temperature at the particle surface can be achieved and the solidification process started.

If the fusion and the solidification of pure metals are considered, the Stefan problem should be solved with the following boundary condition at the liquid/solid interface.

$$T_{p1}(r_i, t) = T_{p2}(r_i, t) = T_{ml} \quad \text{(Eq 24)}$$

The interface movement velocity, dr_i/dt, is determined with the Stefan heat balance condition at the moving interface $r = r_i$, which states that the difference between the heat fluxes associated with both liquid and solid phases is equal to the rate of heat absorption due to melting or to the rate of heat extraction due to solidification (Ref 2, 4):

$$\lambda_{p1}\left(\frac{\partial T_{p1}}{\partial r}\right)_{r=r_i} - \lambda_{p2}\left(\frac{\partial T_{p2}}{\partial r}\right)_{r=r_i} = \chi \rho_{p1} \frac{dr_i}{dt} \quad \text{(Eq 25)}$$

In Ref 3 and 4, the influence of the Knudsen effect both on heat and momentum transfer is shown to be small during HVOF spraying. In this case it is possible to neglect this effect, particularly for powder particles where $d_p = 10$ to 40 μm.

3. Analytical Investigation

3.1 *Momentum Transfer*

In this section, to simplify the mathematics and to clarify the physics of the fluid/particle transport phenomena, we shall consider the fluid properties (ρ_f, μ_f, c_f, and λ_f) to be constant. Within the framework of the general approach, situations corresponding to different values of Reynolds number are considered.

We start with the case $\eta = 0$, where V_f is determined by Eq 1 to 4 and Eq 9, and V_p is found from Eq 15. In creeping flow ($Re < 2$), $c_D = 24/Re$ and from Eq 15:

$$\frac{dV_p}{dt} = a_2(V_f - V_p) \quad \text{(Eq 26)}$$

If V_f = const,

$$V_p = V_f - (V_f - V_{p0})b, b = \exp(-a_2 t) \quad \text{(Eq 27)}$$

The location of the particle is determined from Eq 17 and 27:

$$z = V_f t + a_2^{-1}(V_f - V_{p0})(b - 1) + z_0 \quad \text{(Eq 28)}$$

From Eq 27 it follows that the particle velocity is going to V_f as $t \to \infty$.

In the general case of $V_f = V_f(t)$, Eq 26 yields:

$$V_p = b\left(V_{p0} + a_2 \int_0^t V_f b^{-1} dt\right) \quad \text{(Eq 29)}$$

The particle trajectory is determined by:

$$z = a_2^{-1} V_{p0}(1 - b) + a_2 \int_0^t b dt \int_0^t V_f b^{-1} dt + z_0 \quad \text{(Eq 30)}$$

When V_f = const, we obtain from Eq 29 and 30 the formulas given in Eq 27 and 28, respectively.

In the intermediate region ($2 < Re < 500$), the drag coefficient can be taken approximately as $c_D \approx 18.5 Re^{0.6}$ (Ref 11). Then, from Eq 15:

$$\frac{dV_p}{dt} = A_1(V_f - V_p), A_1 = \frac{13.9\,\rho_f^{0.4}\,\mu_f^{0.6}}{\rho_d d_p^{1.6}} \quad \text{(Eq 31)}$$

If V_f = const, Eq 31 yields:

$$V_p = V_f - [0.4A_1 t + (V_f - V_{p0})^{-0.4}]^{-2.5} \quad \text{(Eq 32)}$$

The particle velocity determined with Eq 32 increases from V_{p0} to V_f with increase in time. The particle location corresponding to Eq 32 is

$$z = z_0 + V_f t + (0.6A_1)^{-1}[0.4A_1 t + (V_f - V_{p0})^{-0.4}]^{-1.5} \quad \text{(Eq 33)}$$

Now we shall consider the general case corresponding to Eq 13, which takes into account the interaction between fluid and powder particles. If $Re < 2$ and $c_D = 24/Re$,

$$\frac{dV_p}{dt} = a_2(1 + \eta)(V_f - V_p) \quad \text{(Eq 34)}$$

When the fluid velocity can be approximated as a constant (V_f = const),

$$V_p = V_f - b_1(V_f - V_{p0}), b_1 = \exp(-\tau_p^{-1} t), \tau_p = [a_2(1 + \eta)]^{-1} \quad \text{(Eq 35)}$$

where τ_p is the particle relaxation time determining its velocity damping due to viscous effects during particle movement. In the absence of fluid/particle interactions ($\eta = 0$), this time is equal to a_2^{-1} and decreases when $\eta \neq 0$. Thus, these interactions enhance particle energy dissipation during HVOF spraying.

When $V_f = V_f(t)$, Eq 34 yields:

$$V_p = b_1 (V_{p0} + \tau_p^{-1} \int_0^t V_f b_1^{-1} dt) \quad \text{(Eq 36)}$$

If $\eta = 0$, we obtain from Eq 35 and 36 the formulas given in Eq 27 and 29, respectively.

In the interval $2 < Re < 500$, the ordinary differential equation (Eq 34) can be reduced to the transcendental equation for V_p, which is then solved using an iterative process.

The fluid/particle interactions also influence fluid velocity. In the case of creeping flow, substituting Eq 27 in Eq 11 yields the following for $V_f^{(1)}$:

$$\frac{dV_f^{(1)}}{dt} = -\frac{a_1 \eta}{1 - \eta}(V_f^{(0)} - V_{p0})b_1 \quad \text{(Eq 37)}$$

Taking $V_f^{(1)} = V_{f0}^{(1)}$ at $t = 0$,

$$V_f^{(1)} = V_{f0}^{(1)} - \eta\, \rho_p \rho_f^{-1}(V_f^{(0)} - V_{p0})(1 - b_1) \quad \text{(Eq 38)}$$

Equation 38 shows that fluid/particle interactions lead to a decrease in fluid velocity. This is particularly important in HVOF and plasma spraying, where $\rho_p \rho_f^{-1} >> 1$ and the fluid velocity decrease due to the particles is rather significant even under very small values of the particle volume fraction, η (Ref 8).

3.2 *Heat Transfer*

Generally, the in-flight thermal behavior of powder particles during HVOF spraying is as follows: melting (partial or complete), cooling, and solidification (partial or complete). It is clear that the final step is highly undesirable from the standpoint of coating quality. The primary challenge in HVOF spraying technology, however, is to obtain the optimal balance between coating quality and processing parameters. Therefore, all possible thermal situations should be investigated.

3.2.1 Particle Heating and Melting

Consider a spherical particle with a radius R_p. The heat Q_p needed to heat and melt the particle volume W is

$$Q_p = \rho_{p2} W c_{p2}(T_{ml} - T_{p0}), W = \frac{4}{3}\pi(R_p^3 - R_{ml}^3) \quad \text{(Eq 39)}$$

The heat Q_s coming to the particle surface $S = 4\pi R_p^2$ due to the heat flux q during the time interval Δt is

$$Q_s = 4\pi R_p^2 q \Delta t, q = \alpha(T_f - T_{ps}) \quad \text{(Eq 40)}$$

From the heat balance condition $Q_p = Q_s$, it follows that:

$$R_{ml} = R_p \sqrt[3]{1 - \beta}, \beta = 3q\Delta t[\rho_{p2} c_{p2} R_p (T_{ml} - T_{p0})]^{-1} \quad \text{(Eq 41)}$$

The thickness δ_m of the melted spherical layer is

$$\delta_{ml} = R_p - R_{ml} = R_p[1 - \sqrt[3]{1 - \beta}] \quad \text{(Eq 42)}$$

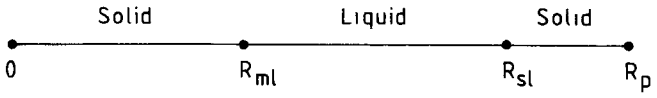

Fig. 2 Radial regions of particle melting and solidification

The value β determines the melted volume fraction of the particle. The complete particle melting corresponds to $R_c = 0$. From Eq 41, it follows that the full melting time t_{ml} is determined by:

$$t_{ml} = \rho_{p2} c_{p2} R_p (T_{ml} - T_{p0})(3q)^{-1} \quad \text{(Eq 43)}$$

In the case of a cylindrical particle where $R_p << h$, $S = 2\pi R_p h$, and $W = \pi h(R_p^2 - R_c^2)$, we obtain from the heat balance condition that:

$$R_c = R_p\sqrt{1-\gamma},\ \gamma = 1.5\beta \quad \text{(Eq 44)}$$

The thickness of the melted layer is

$$\delta_{ml} = R_p(1 - \sqrt{1-\gamma}) \quad \text{(Eq 45)}$$

and the full melting time is

$$\tau_{ml} = 1.5 t_{ml} \quad \text{(Eq 46)}$$

Equations 44 and 46 show that the melted volume fraction β in the spherical case exceeds γ in the cylindrical case and that the full melting time t_m of the spherical particle is smaller than that of the cylindrical particle. Therefore, under the same thermal conditions, the spherical particle has more favorable conditions for heating and melting than the cylindrical particle.

3.2.2 Particle Cooling and Solidification

After melting and further heating, the powder particle can be cooled and solidified if the fluid temperature decreases during HVOF spraying. Let the spherical particle being melted and heated have a heat content of:

$$Q_p = \rho_{p2} c_{p2} W(T_p - T_{ml}) \quad \text{(Eq 47)}$$

The heat Q_s extracted from the particle surface S during the time interval Δt due to the heat flux q determined with the boundary condition given in Eq 20 at the particle surface is

$$Q_s = qS\,\Delta t,\ q = \alpha(T_{ps} - T_f) \quad \text{(Eq 48)}$$

The time Δt_c of the particle cooling up to the solidification temperature is determined from the heat balance condition $Q_p = Q_s$. Thus, from Eq 47 and 48,

$$\Delta t_c = \frac{\rho_{p2} c_{p2}(R_p^3 - R_{ml}^3)(T_p - T_{ml})}{3\alpha R_p^2 (T_{ps} - T_{fa})} \quad \text{(Eq 49)}$$

It is interesting to compare Δt_c with the time Δt_{ml} needed for melting of the same particle volume, which is obtained from Eq 39 and 40:

$$\Delta t_c = \frac{\rho_{p2} c_{p2}(R_p^3 - R_{ml}^3)(T_{ml} - T_{p0})}{3\alpha R_p^2 (T_{fb} - T_{ps})} \quad \text{(Eq 50)}$$

In Eq 49 and 50, the values T_{fa} and T_{fb} denote the fluid temperatures that cool and heat, respectively, the particle surface; thus, $T_{fb} > T_{fa}$. It follows that:

$$\frac{\Delta t_c}{\Delta t_{ml}} = \frac{(T_p - T_{ml})(T_{fb} - T_{ps})}{(T_{ps} - T_{fa})(T_{ml} - T_{p0})} \quad \text{(Eq 51)}$$

In the case of the cylindrical particle,

$$\Delta t_c = \frac{\rho_{p2} c_{p2}(R_p^2 - R_{ml}^2)(T_p - T_{ml})}{2\alpha R_p (T_{ps} - T_{fa})} \quad \text{(Eq 52)}$$

$$\Delta t_{ml} = \frac{\rho_{p2} c_{p2}(R_p^2 - R_{ml}^2)(T_{ml} - T_{p0})}{2\alpha R_p (T_{fb} - T_{ps})} \quad \text{(Eq 53)}$$

The relation between Δt_c and Δt_{ml} is the same as in Eq 51; however, from Eq 49, 50, 52, and 53 it follows that the values of Δt_c and Δt_{ml} for the spherical particle are smaller than the corresponding values for the cylindrical particle, which implies that the thermal process is more intensive in the former case.

Now consider the possible particle solidification as a consequence of the fluid temperature decrease. The scheme of this process is presented in Fig. 2. The heat balance here in the case of a spherical particle is

$$Q_l + Q_k = \alpha S\,\Delta t(T_{ps} - T_f),\ Q_l = \rho_{p2} c_{p2} W(T_p - T_{ml}),$$

$$Q_k = \chi W \rho_{pl},\ \alpha = [\alpha_f^{-1} + \lambda_{pl}^{-1}(R_p - R_{sl})]^{-1} \quad \text{(Eq 54)}$$

From Eq 54, the position of the solidification front ($R = R_{sl}$) is

$$R_{sl} = R_p\sqrt[3]{1-\varepsilon} \quad \text{(Eq 55)}$$

$$\varepsilon = \frac{3\alpha\,\Delta t(T_{ps} - T_f)}{\rho_{p2} R_p[\chi + c_{p2}(T_p - T_{ml})]} \quad \text{(Eq 56)}$$

The value ε determines the solidified volume fraction of the powder particle. The similar relations for the cylindrical particle are

$$R_{sl} = R_p\sqrt{1 - 1.5\varepsilon} \quad \text{(Eq 57)}$$

Here the solidification process is less intensive than for the spherical particle.

4. Mathematical Simulation

The mechanical problem (Eq 13, 14, 16, and 17) was solved numerically with the Runga-Kutta method. The solution of the heat transfer problem (Eq 18 to 25) was obtained using the method of finite differences of the second order in the implicit form with absolute stability. The numerical algorithm is similar to that described in Ref 12 and 13.

The particle behavior of WC-12Co and nickel (d_p = 10 to 40 μm) was investigated. Spray parameters corresponding to the HVOF system installed at the University of Barcelona (Plasma

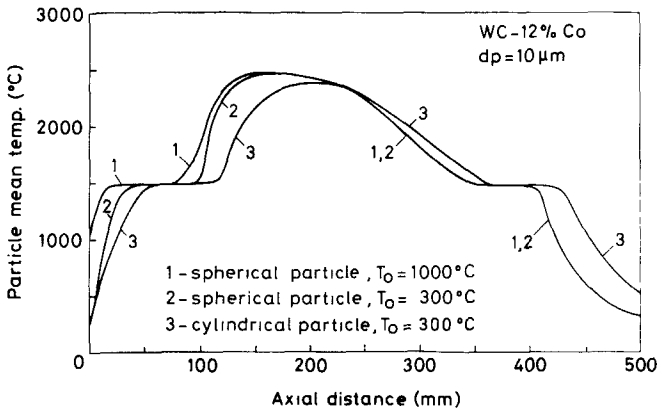

Fig. 3 Variation of mean temperature of WC-12Co spherical and cylindrical particles during HVOF spraying

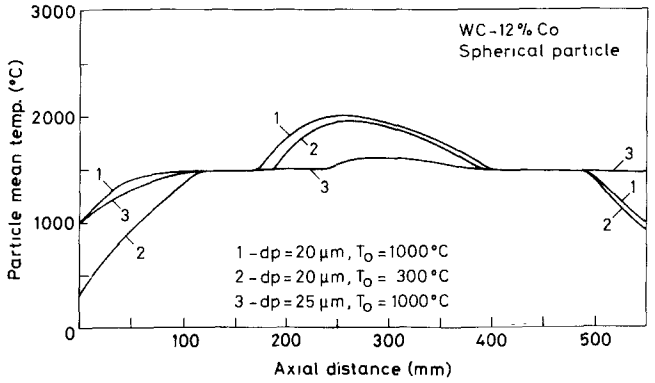

Fig. 4 Variation of mean temperature of WC-12Co spherical particles during HVOF spraying

Technik PT 100) were used: $l = 0.1$ m, $z_m = 0.22$ m, $z_c = 0.4$ m, $L = 0.6$ m, $T_{f0} = 2700$ °C, $T_{fp} = 2600$ °C, $T_{fm} = 2350$ °C, $T_{fc} = 550$ °C, and $T_{fs} = 300$ °C. The parameters of the fluid velocity variations related to particle material were taken according to experimental data and the actual characteristics of the HVOF system (Ref 4).

In accordance with the experimental data, the fluid velocity inside the gun and the fluid temperature inside and outside the gun were calculated using Eq 1 and Eq 5 to 8, respectively. The fluid velocity outside the gun was determined by means of Eq 9.

The properties of the powder materials are given in Table 1 (Ref 7). In the case of WC-12Co, the melting point of cobalt is indicated because only this component of the composite can be melted under HVOF spray conditions. The propane/oxygen ratio was taken to be 1:7 and the combustion gases to consist of carbon dioxide, steam, and unreacted oxygen in the ratio 3:4:2. The thermophysical properties of gases were taken from Ref 14.

5. Results and Discussion

5.1 *Particle Mechanical Behavior*

Powder particle mechanical behavior—without taking into account the fluid/particle interaction ($\eta = 0$)—was studied in detail (Ref 3, 4). The different particle velocities at the spraying

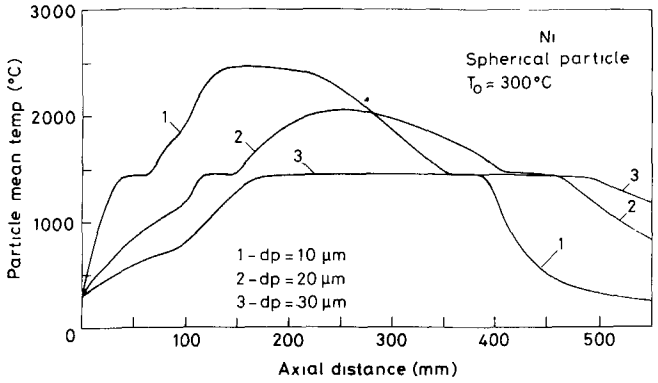

Fig. 5 Variation of mean temperature of nickel spherical particles during HVOF spraying

distance were shown to increase and achieve their maximum values in the region of the combustion flame end and then to decrease in the direction of the substrate surface. The particle density growth leads to a velocity reduction and to the displacement of the particle velocity maximal value in the direction of the substrate. The theoretical results agreed well with the experimental data for the WC-12Co and Al_2O_3 particles (Ref 4, 9).

These results were obtained by numerical integration of the equation of motion (Eq 15), in which the correction factor for c_D is usually introduced to take into account the formation of relatively steep temperature gradients near the particle surface (Ref 2). This correction factor, equal to $(\nu_f/\nu_f)^{0.15}$, is rather artificial without any physical background. Its influence on particle velocity behavior is qualitatively the same as the influence of the fluid/particle interactions, which are taken into account in Eq 13.

The mathematical simulation showed that the results of the numerical integration of Eq 13 are approximately the same as the results of the numerical integration of Eq 15 with the correction factor mentioned earlier. These results are discussed in detail in Ref 3 and 4.

Equations 35 and 38 indicate that the energy dissipation in the fluid/particle mixture caused by the interaction between fluid and powder particles leads to a decrease in the fluid and particle velocities. This effect is amplified with the growth of the particle density. These results have been experimentally confirmed (Ref 9).

5.2 *Particle Thermal Behavior*

The different stages of particle thermal behavior—heating, melting, heating again, cooling, and solidification—were considered by means of mathematical simulation. It is clear that solidification should be avoided during particle in-flight movement in HVOF spraying because it is detrimental to the coating structure. In general, however, the mathematical simulation must also cover this possibility in order to choose the optimal processing version.

During HVOF spraying, the powder particles at first are subjected to heating until they reach their melting point (Fig. 3 to 5). Then, during the melting period, the particle temperature increases slowly as the latent heat of fusion is absorbed. After melting, the particle temperature continues to increase in the

Table 1 Thermophysical properties of powder materials

Property	Nickel	WC-12Co
Density, kg/m^3	8900	14,320
Melting point, K	1727	1768(a)
Heat of fusion, J/kg × 10^6	0.30	0.42
Specific heat, J/kg · K	541	295
Thermal conductivity, W/m · K	73	45

(a) Melting point of cobalt

Table 2 Variations of maximum value of particle mean temperature and its longitudinal position with respect to parameters of WC-12Co particle

d_p, μm	T_0, °C	n	T_m, °C	z_m, m
10	1000	2	2478	0.158
15	1000	2	2319	0.223
20	1000	2	2016	0.252
25	1000	2	1617	0.299
30	1000	2	1495	0.297
10	300	2	2463	0.165
10	100	2	2459	0.167
10	1000	1	2402	0.195
10	300	1	2378	0.207
10	100	1	2372	0.211
20	1000	1	1590	0.296
20	300	2	1958	0.260
20	300	1	1495	0.287

combustion flame up to a maximum near the flame end and then starts to diminish due to the fluid temperature decrease.

The particle temperature finally attains the solidification point, which is equal to the melting point for the pure metals under consideration. During the solidification process, the particle is cooled very slowly despite the significant decrease of the fluid temperature due to the latent heat extraction. This is a characteristic feature during the solidification of metal drops, particularly during metal atomization (Ref 15, 16).

Particle heating after fusion is weakened with particle size enhancement and is rather small for particles where $d_p = 30$ μm, compared with $d_p = 20$ μm and especially $d_p = 10$ μm. The maximum of the particle temperature is displaced in the direction of the substrate surface as particle diameter increases.

The influence of the particle initial temperature growth leading to the particle temperature increase is most important during heating before melting for relatively small particles and diminishes as d_p increases. With the particle size enhancement, the initial temperature influence becomes more important in the region of the particle temperature maximum due to thermal inertia.

As discussed earlier, the thermal processes in cylindrical particles are less intensive than in spherical particles. Therefore, the temperature of cylindrical particles is lower during heating and higher during cooling than the temperature of spherical particles of the same diameter (Fig. 3), and thus the spraying distance for cylindrical particles can exceed that for same-size spherical particles.

Comparison of Fig. 3 to 5 shows that the periods of fusion and solidification of nickel particles are shorter than those of

Table 3 Variations of maximum value of particle mean temperature and its longitudinal position with respect to parameters of nickel particle

d_p, μm	T_0, °C	n	T_m, °C	z_m, m
20	300	2	2055	0.252
20	300	1	1723	0.283
10	300	2	2472	0.160
10	1000	2	2489	0.153
20	1000	2	2171	0.240
30	1000	2	1728	0.290
40	1000	2	1455	0.297

WC-12Co particles. This is because the latent heat of fusion in the first case is smaller than in the second case. The heat diffusivity of nickel exceeds that of WC-12Co; as a result, the maximum temperature for nickel particles occurs earlier and its value is higher. This difference amplifies with increased particle diameter.

The particle maximum temperature T_m and its position z_m, which are of significant interest in HVOF spraying, are presented in Tables 2 and 3. The particle diameter growth causes a decrease in T_m and an increase in z_m due to enhancement of the thermal inertial effects. The maximum temperature grows and its longitudinal coordinate diminishes with increased particle initial temperature.

The same tendencies occur for cylindrical particles, but here the maximum temperatures are lower and the distances z_m are longer than in the case of spherical particles. Also, the differences between the values of T_m characterizing the thermal states of the cylindrical particles with different diameters and initial temperatures are higher than the corresponding differences for the spherical particles. In the case of nickel particles, the values of T_m are higher and the values of z_m are smaller than for WC-12Co particles.

The analytical formulas obtained previously can also be used to approximately predict powder particle thermal behavior. One of the important parameters is the full melting time determined using Eq 43. If $R_p = 10^{-5}$ m, $\rho_{p2} = 14{,}320$ kg/m^3, $c_{p2} = 295$ J/kg · K, $T_{ml} - T_{p0} = 1195$ °C, $T_f - T_{ps} = 1800$ °C, and $\alpha = 19{,}500$ W/m^2 · K, which correspond to the thermal state of WC-12Co particles in HVOF spraying, we find that $t_{ml} \approx 4.8 \times 10^{-4}$ s. From the data presented in Fig. 4 (curve 2), it follows that $t_{ml} \approx 5.7 \times 10^{-4}$ s. The difference between these two values of t_{ml} is quite reasonable.

The same analysis refers to the comparison of the thermal behavior of spherical and cylindrical particles. From the numerical results, it follows that the full melting time of the cylindrical particles τ_{ml} is approximately 1.6 times higher than that of the spherical particles. This agrees well with the analytical prediction made in Eq 46, where $\tau_{ml} = 1.5\, t_{ml}$.

Using Eq 51, if $T_{ml} - T_{p0} = 1195$ °C, $T_{fb} - T_{ps} = 1800$ °C, $T_p - T_{ml} = 970$ °C, and $T_{ps} - T_{fa} = 400$ °C, which corresponds to the thermal behavior of the spherical particle of WC-12Co with $d_p = 10$ μm presented in Fig. 3 (curve 2), we obtain $\Delta t_c/\Delta t_{ml} \approx 3.65$. In accordance with the numerical results, we have $\Delta t_c/\Delta t_{ml} \approx 3.28$. The agreement between these two values is good.

Based on a comparison of the presented results, the spraying distance for the relatively small particles ($d_p = 10$ μm) should be no smaller than about 400 mm, whereas for larger particles ($d_p =$

20 μm) this distance can be increased up to about 480 μm and, in the case where d_p = 25 μm, can exceed 500 μm. Thus, the maximum spraying distance increases with particle weight (and size in the case of similar particles). This occurs because the weight increase causes a particle velocity decrease and hence an enhancement of its residence time under the elevated temperatures. The interval of the permissible spraying distances also increases with particle weight.

In the case of cylindrical particles, the maximum spraying distance is greater than for spherical particles. This increase in spraying distance with a decrease in particle surface curvature is due to retardation of thermal-induced processes. It is also worth noting that a similar situation can occur for spherical particles if their shape is subjected to the in-flight change, particularly with regard to elongation (Ref 17).

In general, it is clear that the particle temperature corresponding to the optimal conditions of metal deposition on the substrate surface should be a bit higher than the powder material melting point. In the case of WC-Co particles, it must exceed the melting point of cobalt. Figures 3 to 5 show that these optimal conditions can be realized more easily for particle diameters in the interval of 20 to 40 μm, which is recommended for WC-Co and nickel particles by manufacturers of HVOF spray equipment (Ref 9). Particles of significantly greater size may not melt as well. Those of smaller diameter (e.g., 10 μm) have a close tolerance for the optimal spraying distance. Beyond this distance, the particle is supercooled. If the spraying distance is smaller than the optimal distance, the particles of the powder materials considered here reach the substrate surface in the superheated liquid state, which causes excessive metal loss and irregular coating formation. Thus, coating quality depends significantly on the choice of optimal spraying distance (Ref 18 to 20).

The presented mathematical model generally can account for particle mass decreases due to evaporation. This mass loss can be taken into account by the term $-m_p V_p dm_p/dt$ on the right side of the equation of motion (Eq 13) and leads to an increase in particle velocity, which can be estimated as follows.

Consider creeping flow when $\eta = 0$. By placing the above-mentioned term in Eq 15, we obtain its solution in the form:

$$V_p = m_p^{-1} b \left(m_{p0} V_{p0} + a_2 \int_0^t V_f m_p b^{-1} dt \right) \quad \text{(Eq 58)}$$

When the particle mass is constant ($m_p = m_{p0}$), Eq 58 yields Eq 29.

The mass loss is determined with the evaporation reactions at the particle surface (Langmuir evaporation) and mass transfer across the boundary layer. These phenomena can be taken into account with the overall mass transfer coefficient, which is equal to the combination of the rate coefficient for Langmuir evaporation and the mass transfer coefficient obtained from another Ranz-Marshall equation similar to Eq 22 (Ref 21).

For our purposes, it is enough to represent m_p as:

$$m_p = m_{p0} \exp(-ct) \quad \text{(Eq 59)}$$

where c^{-1} is the characteristic time of the particle mass loss determined with the mentioned phenomena.

When V_f = const, Eq 58 and 59 yield:

$$V_p = a_2 b_2^{-1} V_f - (a_2 b_2 V_f - V_{p0}) \exp(-b_2 t),\ b_2 = a_2 - c \quad \text{(Eq 60)}$$

Comparison of Eq 60 and 27 shows that the particle mass decrease causes a velocity increase and an increase in characteristic time of V_p change that is equal to b_2^{-1}. The influence of this mass loss on the particle thermal state is more complicated because it leads to the temperature increase caused by the decrease in particle size, which must compete with the particle energy loss due to the extraction of latent heat of vaporization as well as the mass loss.

Under the thermal conditions of HVOF spraying, the particle temperature is well below the boiling points of the powder materials, particularly those of cobalt (2900 °C) and nickel (2730 °C). The corresponding vapor pressures, P_v, are very small. In the case of the nickel particles, for example, P_v varies from 1.3 $\times 10^{-3}$ to 0.13 bar in the temperature interval from 1810 to 2364 °C (Ref 14). Thus, the powder particle mass loss can be neglected unless the particles are extremely small. On the other hand, this factor must be taken into account in plasma spraying, where the processing temperatures are much higher than in HVOF spraying.

6. Conclusions

A mathematical model that describes both mechanical and thermal behavior of powder particles during HVOF thermal spraying is presented. The model takes into account the fluid/solid particle interactions and the full thermal evolution of the particles, including their heating, melting, cooling, and possible solidification, as well as their morphology. Analytical formulas are obtained that describe the approximate particle mechanical and thermal behavior. The energy dissipation in the fluid/solid particle mixture caused by interactions between fluid and powder particles leads to a decrease in fluid and particle velocities, which is amplified as particle density increases.

During HVOF spraying, the powder particles at first are heated to their melting point. Then, in the melting period, the particle temperature increases slowly. After melting, the particle temperature increases up to its maximum value in the region of the combustion flame end and then starts to diminish until attaining the solidification point. During solidification, the particles cool slowly; after solidification, the cooling effect becomes more pronounced. An increase in particle size lessens the effect of particle heating after fusion and causes the displacement of the particle temperature maximum in the direction of the substrate surface.

The influence of the initial temperature growth of the particle is most important during the heat phase prior to melting for relatively small particles. This influence diminishes with an increase in particle size.

The thermal processes in cylindrical particles are less intensive than in spherical particles because of decreased particle surface curvature. As a result, the temperature of cylindrical particles is lower during heating and higher during cooling than the temperature of spherical particles of the same size.

The periods of fusion and solidification of nickel particles are shorter than those of WC-12Co particles. The maximum temperature for nickel particles occurs earlier and its value is higher than in the case of WC-12Co. This difference increases with particle diameter.

The maximum temperature of the particle decreases with increased particle size and decreased initial temperature. The position of the particle maximum temperature is displaced forward as the particle size increases and its initial temperature decreases.

Similar tendencies occur for cylindrical particles, but here the values of T_m are smaller and those of z_m are greater than in the case of spherical particles. The values of T_m are higher and the values of z_m are smaller for the nickel particles compared with similar values for WC-12Co particles.

The maximum spraying distance and the interval of the permissible spraying distances increase with particle size. For cylindrical particles, the maximum spraying distance is greater than for spherical particles. The cylindrical particle form is generally more useful than the spherical form.

The optimal thermal conditions of HVOF spraying of the powders considered can be more easily achieved for particle diameters from 20 to 40 μm. The tolerance for the optimal spraying distance becomes more stringent with a decrease in particle size. The supercooling or possible superheating of the particles with larger or smaller diameters diminishes coating quality. The mathematical model can be used to predict powder particle behavior during HVOF spraying to obtain the optimal coating structure (Ref 18 to 20).

Acknowledgments

The authors express their gratitude to Generalitat de Catalunya for financial support received (project GRQ93-1017) and to Plasma Technik AG for cooperation and useful discussions. V.V. Sobolev also thanks CICYT for the concession of the sabbatical year SAB 94-0066 in the University of Barcelona. J.A. Calero is grateful to Generalitat de Catalunya for the concession of an F.I. grant.

References

1. M.L. Thorpe and H.J. Richter, A Pragmatic Analysis and Comparison of HVOF Processes, *J. Therm. Spray Technol.*, Vol 1 (No. 2), 1992, p 161-170
2. A. Apelian, M. Paliwal, R.W. Smith, and W.F. Schilling, Melting and Solidification in Plasma Spray Deposition—Phenomenological Review, *Int. Met. Rev.*, Vol 28 (No. 5), 1983, p 271-294
3. V.V. Sobolev, J.M. Guilemany, and J.A. Calero, Simulación del Comportamiento de las Particulas de Polvo en el Proceso de Obtención de Recubrimientos mediante Proyección Térmica de Alta Velocidad (HVOF), *Deform. Met.*, No. 216, 1994, p 25-31 (in Spanish)
4. V.V. Sobolev, J.M. Guilemany, J.C. Garmier, and J.A. Calero, Modelling of Particle Movement and Thermal Behaviour during High Velocity Oxy-fuel Spraying, *Surf. Coat. Technol.*, Vol 63, 1994, p 181-187
5. P. Fauchais, A. Vardelle, and M. Vardelle, Modelling of Plasma Spraying of Ceramic Coatings at Atmospheric Pressure, *Ceram. Int.*, Vol 17, 1991, p 367-378
6. E. Pfender, Particle Behaviour in Thermal Plasmas, *Plasma Chem. Plasma Process.*, Vol 9 (No. 1), 1989, p 167s-194s
7. S.V. Joshi and R. Sivakumar, Particle Behaviour during High-Velocity Oxy-fuel Spraying, *Surf. Coat. Technol.*, Vol 50, 1991, p 67-74

Nomenclature

A	coefficient of equation, ms^{-1}
B	coefficient of equation, s^{-1}
c	specific heat, J/kg · K
c_D	drag coefficient
C	coefficient of equation, ms^{-1}
d	diameter, m
h	cylindrical particle length, m
l	gun length, m
L	gun length plus spraying distance, m
n	factor of geometry; $n = 1, 2$ corresponds to cylindrical and spherical geometries, respectively
Nu	Nusselt number
Pr	Prandtl number
q	heat flux, W/m^2
Q	heat, J
r	radial coordinate, m
R	radius, m
Re	Reynolds number
S	particle surface, m^2
t	time, s
Δt	time interval, s
T	temperature, °C
V	velocity, m/s
W	volume, m^3
z	longitudinal coordinate, m

Greek Letters

α	heat transfer coefficient, $W/m^2 \cdot K$
β	melted volume fraction of spherical particle
γ	melted volume fraction of cylindrical particle
δ	thickness of melted layer, m
ε	solidified volume fraction of spherical particle
η	solid particle volume fraction
λ	thermal conductivity, W/m · K
μ	viscosity, kg/m · s
ν	kinematic viscosity, m^2/s
ρ	density, kg/m^3
τ	relaxation time
φ	particle sphericity
χ	latent heat of fusion, J/kg

Subscripts

c	cooling
f	fluid
i	interface
m	maximal
ml	melting
p	particle
s	particle surface
sl	solidification
0	initial
1	solid
2	liquid

8. K.S. Han, M.K. Chung, and H.J. Sung, Application of Lumley's Drag Reduction Model to Two-Phase Gas-Particle Flow in a Pipe, *Trans. ASME, J. Fluids Eng.*, Vol 113, 1991, p 130-136
9. *Introduction to the CDS Technology,* Plasma Technik AG, Wohlen, 1990, p 4-7
10. R. Clift, J.R. Grace, and M.E. Weber, *Bubbles, Drops and Particles,* Academic Press, 1978, p 69-219
11. J. Szekeley and N. Themelis, *Rate Phenomena in Process Metallurgy,* Wiley-Interscience, 1971, p 601-637
12. V.V. Sobolev and P.M. Trefilov, *Thermophysics of Metal Solidification during Continuous Casting,* Metallurgy, Moscow, 1988, p 80-128 (in Russian)
13. V.V. Sobolev and P.M. Trefilov, *Optimization of Thermal Conditions of Melts Solidification,* University Press, Krasnoyarsk, 1986, p 91-106 (in Russian)
14. V. Dembowsky, *Plasma Metallurgy: The Principles,* Elsevier, Amsterdam, 1985, p 115-180
15. V.V. Sobolev and N.A. Nesterov, Structure Formation in Granules during Crystallization, *Sov. Powder Metall.*, No. 11, 1989, p 1-6
16. V.V. Sobolev and N.A. Nesterov, Kinetics of Alloy Crystallization during Granulation of Metals, *Nonferrous Met.*, No. 12, 1988, p 67-70
17. G. Trapaga and J. Szekeley, Mathematical Modelling of the Isothermal Impingement of Liquid Droplets in Spraying Processes, *Metall. Trans. B,* Vol 22B, 1991, p 901-914
18. J.M. Guilemany, N. Llorca-Isern, and J. Nutting, Ceramic Coatings Obtained by Means of HVOF Thermal Spraying, *Powder Metall. Int.*, Vol 25 (No. 4), 1993, p 176-179
19. V.V. Sobolev and J.M. Guilemany, Investigation of Coating Porosity Formation during High Velocity Oxy-fuel (HVOF) Spraying, *Mater. Lett.*, Vol 18, 1994, p 304-308
20. J.M. Guilemany, V.V. Sobolev, J. Nutting, Z. Dong, and J.A. Calero, Thermal Interaction between WC-Co Coating and Steel Substrate in Process of HVOF Spraying, *Scr. Metall. Mater.*, Vol 31 (No. 7), 1994, p 915-920
21. R. Westhoff, G. Trapaga, and J. Szekeley, Plasma-Particle Interactions in Plasma Spraying Systems, *Metall. Trans.*, Vol 23B, 1992, p 683-693